

Active Microwave Cloaking Using Parity-Time-Symmetric Satellites


Ahmed Kord,¹ Dimitrios L. Sounas,¹ and Andrea Alù^{1,2,3,4,*}

¹*Department of Electrical and Computer Engineering, the University of Texas at Austin, Austin, Texas 78712, USA*

²*Photonics Initiative, Advanced Science Research Center, City University of New York, New York, New York 10031, USA*

³*Physics Program, Graduate Center, City University of New York, New York, New York 10026, USA*

⁴*Department of Electrical Engineering, City College of New York, New York, New York 10031, USA*

 (Received 11 July 2018; revised manuscript received 11 October 2018; published 19 November 2018)

In this paper, we present and study the dynamics of an active microwave cloaking technique that alleviates the trade-offs between loss, bandwidth, and size inherent in passive approaches. The presented cloak consists of a finite number of satellite antennas loaded with parity-time-symmetric lumped admittances, which, without external control, can track in real time the amplitude, frequency, and phase variations of the impinging signals and generate the required current distributions at the antennas to totally suppress the scattered waves, including reflections and shadows. We analytically derive the optimal density and frequency dispersion of the antenna satellites surrounding the object in order to achieve substantial reduction in the scattering crosssection over a wide bandwidth. We also investigate the conditions necessary to maintain the cloak stability and study its transient response for excitation with pulsed signals.

DOI: [10.1103/PhysRevApplied.10.054040](https://doi.org/10.1103/PhysRevApplied.10.054040)

I. INTRODUCTION

The possibility of minimizing the scattering from an object and making it undetectable to external observers has intrigued the imagination of mankind for centuries. This process, known in the scientific literature as cloaking [1–10], is not only of fundamental significance from a basic research standpoint, but it can also enable new applications in different portions of the electromagnetic spectrum, including microwaves and optics, and even in other physical domains, namely, acoustics, mechanics, and thermodynamics. In the microwave regime, which is the main focus of this paper, potential applications include reducing the interference between multiantenna radio systems as in next-generation massive multiple-input multiple-output (MIMO) wireless communication systems [11–13], advancement of stealth technology in radar systems to suppress the shadow of hidden objects [14,15], and improving the efficiency of radio-frequency energy harvesting by eliminating the loss due to scattering [16–18]. Research in this area has seen different breakthroughs since the advent of metamaterials and numerous approaches to cloaking have been explored, including transformation optics [1,2], carpet cloaking [3], mantle cloaking [4,5], plasmonic cloaking [6,7], and a few others [8–10]. Yet, several challenges hinder all these approaches, including the loss that inevitably accompanies the dispersion of

metamaterials [19] and the difficulty of achieving large scattering suppression over a sufficiently wide bandwidth (BW), especially for arbitrarily shaped large objects [20, 21]. Overcoming these limitations without compromising other specifications of the target application is a necessity for cloaking technologies to become relevant in practical scenarios. For example, covering an object with an elongated hard surface [22] may provide broadband scattering reduction for one polarization of interest, thus overcoming the bandwidth problem, but the increase in size may be unacceptable in mobile communication systems. Consequently, these challenges have cast doubts on whether cloaking can really escape the realm of basic research and become a technological reality.

Interestingly, a common assumption in the vast majority of cloaking techniques proposed to date is the use of only passive materials. In Ref. [21], it was shown that independent of the adopted scheme, passive and linear cloaks are always subject to stringent upper bounds on the operational bandwidth, which become more and more stringent as the object size increases. These bounds suggest that practical broadband cloaking can only be feasible with the adoption of active devices. A few attempts toward this goal have been investigated in the last few years [23–27]. In particular, [23] proposed the idea of using an array of sensors to measure the fields around the object being concealed, then processing the measured values to calculate the required signals that need to be applied to a set of radiating sources to cancel the scattered waves. The main challenge with

*aalu@gc.cuny.edu

this approach, however, is that the delay related to sensing and postprocessing of the measured signals needs to be small compared to the time taken for the wave to propagate through the cloaked volume. As explained in Ref. [23], this may be possible for slowly propagating waves, as in acoustics, for which information can be transmitted at higher speeds around the cloaked volume via electrical or optical networks, but it may be quite challenging for electromagnetic waves. This problem can be overcome to some extent in applications where the angle of incidence is restricted within a particular range, a situation commonly referred to as unidirectional cloaking [28–30]. In such a case, it would be sufficient to have a local and separate feedback network for each source, instead of a nonlocal joint feedback network between all sources, as is necessary in the case of omnidirectional cloaking. Toward this direction, [24] proposed and experimentally demonstrated unidirectional cloaking at microwave frequencies through a finite number of sources externally driven by independent signal generators. However, this process required prior knowledge of the incident wave characteristics, i.e., amplitude, phase, and frequency information, which, for realistic scenarios where the incident wave is modulated in time, implies the necessity of advanced sensors in front of the object that can track the rapidly changing incident wave.

In order to overcome this problem, [25] presented an active cloaking technique inspired by the concept of parity-time (PT) symmetry. This special form of symmetry, originally introduced in quantum mechanics [31–33] and recently extended to optics and electromagnetics [34–36], concerns structures that are symmetric upon a concurrent inversion of spatial and time coordinates. In optics, this situation corresponds to systems with spatially balanced loss and gain. Applying this concept to electromagnetic (EM) scattering problems has led to a new class of unidirectional cloaks in which PT symmetry implies covering the object with a surface having a balanced distribution of loss and gain. The impedance of this surface is appropriately selected to absorb the incident wave from one side, as in conventional stealth devices, and then reemit it on the other side, thus cancelling the shadow that always exists in passive stealth devices and achieving total invisibility. To introduce this concept, [25] explored a rather unrealistic metasurface model with a continuously varying admittance profile, which cannot be implemented in practice.

In this paper, we present practical designs of PT symmetric microwave cloaks, consisting of arrays of antenna satellites that surpass the passive metamaterial approaches proposed to date in performance and provide several advantages compared to the available active cloaks, such as increased operational BW and automatic generation of the required signals at the radiating antennas through a fast and stable “analoglike” feedback. Our approach is based on surrounding the scattering object with a finite number of antennas loaded with PT symmetric circuits [26], which

can be implemented using discrete or integrated circuits. We rigorously derive the optimal parameters of these elements, including their number and frequency dispersion, to achieve a set of given specifications that include the level of scattering reduction and operational bandwidth, making sure that the system is stable. We apply the proposed approach to objects with sizes of the order of the wavelength and show that the achieved bandwidth satisfies the requirements of various microwave applications involving realistic digitally modulated signals. Furthermore, we show that the bandwidth of our approach can be significantly larger than the bandwidth of most common passive cloaks based on azimuthally symmetric covers, opening a new venue in the quest toward practical cloaks for broadband signals and large scatterers.

II. FREQUENCY-DOMAIN ANALYSIS

Although the proposed technique can be applied to objects of any shape, for simplicity, our analysis will focus on circularly symmetric perfectly electric conducting (PEC) cylinders with translational invariance along the z axis. A general discussion about how the analysis can be extended to any object and considering any kind of parasitics is provided in the Conclusions. Figure 1 shows the geometry of the problem, a PEC cylinder with radius a , surrounded by N discrete thin wires (satellites), periodically loaded with lumped admittances $Y_{L,k}$ at radius r_c and equidistantly distributed at angles $\phi_k = (k-1)2\pi/N$, where $k = 1 : N$ is an integer that represents the wire index. If the distance d between adjacent lumped admittances is much smaller than the wavelength, the loaded wires can be modeled through the homogenized boundary condition $I_k = Y_k E_k$, where I_k is the current flowing through the k th wire, E_k is the z directed electric field (the electric field parallel to the wires) at the site of the k th wire, and $Y_k = Y_{L,k}d$ is defined as the loaded wire admittance. The unit for Y_k is $(\Omega \text{ m})^{-1}$. For short-circuited

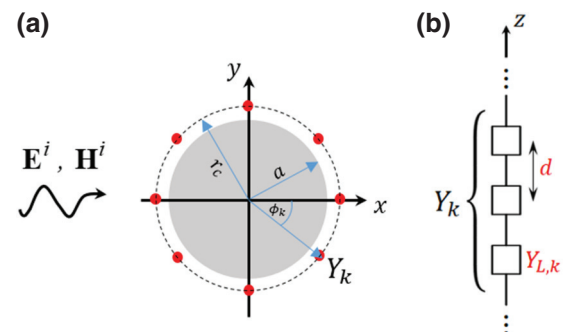


FIG. 1. TM^z plane-wave incidence on a circular PEC cylinder surrounded by N satellite antennas with wire admittance Y_k . (a) Geometry of the problem. (b) Implementation of the satellite antennas as thin wires periodically loaded with lumped admittance $Y_{L,k}$.

wires, i.e., for $Y_{L,k} \rightarrow \infty$, this boundary condition becomes $E_k = 0$, which is simply the boundary condition for a perfectly metallic surface. The satellites play the joint role of sensor/source pairs, where the wire admittance provides a feedback mechanism that is necessary to create signals that cancel the scattered field by the cylinder, as we will explain in the next section. It is worth mentioning at this point that the cross-coupling between all elements, particularly between the active and passive sides, is not only taken into account in the following analysis, but it is also essential to maintain the system's stability, as will be explained in Sec. III.

Now consider an impinging transverse-magnetic (TM^F) wave with an electric field along the z axis propagating along the $+x$ axis with a center frequency f_0 , free-space wavelength and wavenumber λ_0 and β_0 , respectively, and electric field amplitude E_0 , as follows:

$$E^{\text{inc}}(\rho, \phi) = E_0 e^{-j\beta_0 x} = E_0 \sum_{n=-\infty}^{\infty} j^{-n} J_n(\beta_0 \rho) e^{jn\phi}, \quad (1)$$

where $J_n(x)$ is the Bessel function of the first kind and n th order and the unit vector \hat{z} is omitted for simplicity. Our goal is to find the number of satellites N and the optimal values of the wire admittances Y_k , which, for a given frequency f_0 , minimize the normalized scattering coefficient $\overline{\text{RCS}} = \overline{\sigma}_c / \overline{\sigma}_b$, defined as the ratio between the scattering crosssections of the cloaked structure $\overline{\sigma}_c$ and the bare cylinder $\overline{\sigma}_b$, respectively, given by

$$\overline{\sigma}_c = \frac{1}{2\pi} \int \lim_{\rho \rightarrow \infty} \frac{|E^{s,c}(\rho, \phi)|^2}{|E_0|^2} 2\pi \rho d\phi, \quad (2)$$

$$\overline{\sigma}_b = \frac{1}{2\pi} \int \lim_{\rho \rightarrow \infty} \frac{|E^{s,b}(\rho, \phi)|^2}{|E_0|^2} 2\pi \rho d\phi, \quad (3)$$

where $E^{s,b}$ and $E^{s,c}$ are the scattered fields from the bare cylinder and the cloaked structure, respectively. These fields can be found as [37]

$$E^{s,b}(\rho, \phi) = E_0 \sum_{n=-\infty}^{\infty} j^{-n} \frac{J_n(\beta_0 a)}{H_n^{(2)}(\beta_0 a)} H_n^{(2)}(\beta_0 \rho) e^{jn\phi}, \quad (4)$$

$$E^{s,c}(\rho, \phi) = E_0 \sum_{n=-\infty}^{\infty} j^{-n} \frac{J_n(\beta_0 a)}{H_n^{(2)}(\beta_0 a)} H_n^{(2)}(\beta_0 \rho) e^{jn\phi} - \frac{\beta_0 \eta_0}{4} \sum_{k=1}^N I_k \begin{cases} \sum_{n=-\infty}^{\infty} H_n^{(2)}(\beta_0 r_c) \left[J_n(\beta_0 \rho) - \frac{J_n(\beta_0 a)}{H_n^{(2)}(\beta_0 a)} H_n^{(2)}(\beta_0 \rho) \right] e^{jn(\phi - \phi_k)}, & a \leq \rho \leq r_c, \\ \sum_{n=-\infty}^{\infty} H_n^{(2)}(\beta_0 \rho) \left[J_n(\beta_0 r_c) - \frac{J_n(\beta_0 a)}{H_n^{(2)}(\beta_0 a)} H_n^{(2)}(\beta_0 r_c) \right] e^{jn(\phi - \phi_k)}, & \rho \geq r_c, \end{cases} \quad (5)$$

where $H_n^{(2)}(x)$ is the Hankel function of the second kind and n th order, $\eta_0 = 120 \pi \Omega$ is the free-space intrinsic impedance, and I_k is the current flowing through the k th wire. The first term in the right-hand side of $E^{s,c}$ is the scattered field from the bare cylinder, while the second term is the radiated field of the cloaking satellites in the presence of the cylinder. The total fields $E^{\text{tot},b}$ and $E^{\text{tot},c}$ with and without cloaking, respectively, can be calculated using a simple superposition of Eqs. (1), (4), and (5):

$$E^{\text{tot},b} = E^{\text{inc}} + E^{s,b}, \quad (6)$$

$$E^{\text{tot},c} = E^{\text{inc}} + E^{s,c}. \quad (7)$$

In the far-field (FF) region, Eq. (5) can be simplified into

$$E_{\text{FF}}^{s,c}(\rho, \phi) = \sum_{n=-\infty}^{\infty} \left(l_n + X_n \sum_{k=1}^N I_k e^{-jn\phi_k} \right) e^{jn\phi} \frac{e^{-j\beta_0 \rho}}{\sqrt{\rho}}, \quad (8)$$

where l_n and X_n are two constants given by

$$l_n = -E_0 \sqrt{\frac{2j}{\pi \beta_0}} \frac{J_n(\beta_0 a)}{H_n^{(2)}(\beta_0 a)}, \quad (9)$$

$$X_n = -\frac{\beta_0 \eta_0}{4} \sqrt{\frac{2j}{\pi \beta_0}} j^n \left[J_n(\beta_0 r_c) - \frac{J_n(\beta_0 a)}{H_n^{(2)}(\beta_0 a)} H_n^{(2)}(\beta_0 r_c) \right]. \quad (10)$$

Then the total scattered power is given by

$$P^s = \int_0^{2\pi} \frac{|E_{FF}^{s,c}|^2}{2\eta_0} \rho d\phi = \sum_{n=-\infty}^{\infty} P_n^s$$

$$= \frac{\pi}{\eta_0} \sum_{n=-\infty}^{\infty} \left| l_n + X_n \sum_{k=1}^N I_k e^{-jn\phi_k} \right|^2, \quad (11)$$

where P_n^s is the scattered power corresponding to the n th harmonic. Before calculating the optimal Y_k , we calculate the values of I_k that minimize P^s and subsequently $\overline{\text{RCS}}$. Knowing I_k , the optimal wire admittances can be calculated with $Y_k = I_k/E_k$.

In order to minimize P^s , we take the derivative of Eq. (11) with respect to the real (I'_k) and imaginary (I''_k) parts of I_k to be equal to zero,

$$\frac{\partial P^s}{\partial I'_m} = \sum_{n=-\infty}^{\infty} \frac{\partial P_n^s}{\partial I'_m}$$

$$= 2 \operatorname{Re} \left\{ \sum_{n=-\infty}^{\infty} l_n X_n^* e^{jn\phi_m} + \sum_{k=1}^N l_k \sum_{n=-\infty}^{\infty} |X_n|^2 e^{jn(\phi_m - \phi_k)} \right\} = 0,$$

$$\frac{\partial P^s}{\partial I''_m} = \sum_{n=-\infty}^{\infty} \frac{\partial P_n^s}{\partial I''_m}$$

$$= -2j \operatorname{Im} \left\{ \sum_{n=-\infty}^{\infty} l_n X_n^* e^{jn\phi_m} + \sum_{k=1}^N l_k \sum_{n=-\infty}^{\infty} |X_n|^2 e^{jn(\phi_m - \phi_k)} \right\} = 0. \quad (12)$$

Equation (12) can be formulated into the linear system of equations $\overline{\overline{G}}\overline{\overline{I}} = -\overline{\overline{F}}$, where $\overline{\overline{I}}|_{N \times 1}$ is a column vector of the currents I_k and the elements of $\overline{\overline{G}}|_{N \times N}$ and $\overline{\overline{F}}|_{N \times 1}$ are, respectively, given by

$$g_{mk} = \sum_{n=-\infty}^{\infty} |X_n|^2 e^{jn(\phi_m - \phi_k)}, \quad (13)$$

$$f_m = \sum_{n=-\infty}^{\infty} l_n X_n^* e^{jn\phi_m}. \quad (14)$$

Solving this linear system of equations numerically, we find the optimal currents I_k that minimize the scattered power and scattering crosssection at f_0 . As an example, Fig. 2 presents I_k for a cylinder with $a = \lambda_0/2$, $r_c = a + 0.05\lambda_0$, and $N = 10$, which, as we will see later, leads to

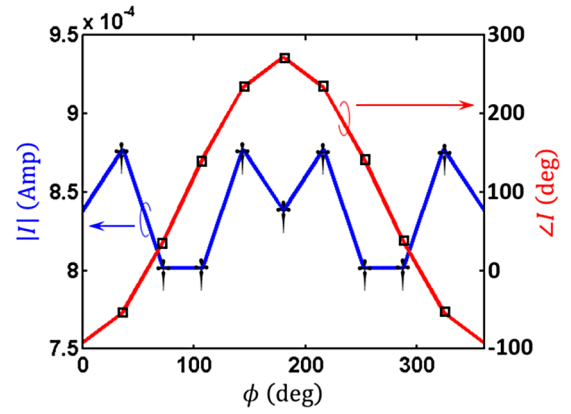


FIG. 2. Optimal current distribution at f_0 to achieve $\overline{\text{RCS}} = -30$ dB for $a = \lambda_0/2$, $r_c = a + 0.05\lambda_0$, and $N = 10$.

a scattering reduction of 30 dB. By substituting the values of I_k into Eq. (11), we can calculate P^s and subsequently $\overline{\text{RCS}}$. Figure 3 shows $\overline{\text{RCS}}$ vs the number of elements N for different radii of the PEC cylinder. As we can see, a larger size requires more satellites to maintain the same level of scattering reduction. Figure 3 also shows that, for a cylinder of a particular size, the scattering reduction improves as the number of satellites increases. However, there are two distinct regions with different slopes of $\overline{\text{RCS}}$ vs N . The transition between the two regions happens approximately when the distance between neighboring satellites is $\lambda_0/2$, as seen in Fig. 3.

This interesting behavior can be understood through the properties of planar surfaces consisting of periodic arrays of particles, which can locally approximate the cloak under study. In particular, if the distance between elements is larger than $\lambda_0/2$, there is a range of incident angles, close to grazing, for which the satellites scatter multiple diffraction orders, making full absorption of the incident wave from one side and reemission from the other one impossible,

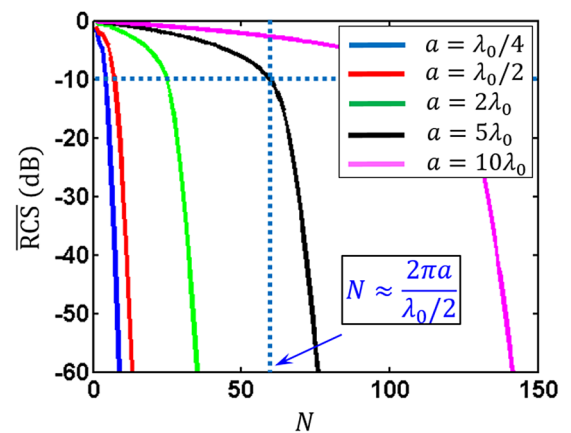


FIG. 3. Normalized scattering coefficient $\overline{\text{RCS}}$ vs the number of satellites N for different sizes of the PEC cylinder.

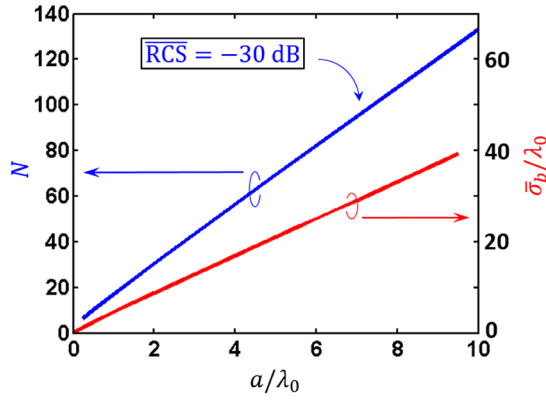


FIG. 4. Uncloaked scattering crosssection $\bar{\sigma}_b$ and the required number of satellites N to achieve $\overline{\text{RCS}} = -30$ dB vs the size of the PEC cylinder.

since a portion of the incident power will be distributed to diffraction orders other than the one associated with the incident plane wave. This problem disappears for a distance smaller than $\lambda_0/2$. In such a case, the higher diffraction orders are evanescent, and the cloak can be designed to perfectly absorb incident waves from a given direction. Perfect invisibility can be achieved only with a continuous impedance profile, i.e., for $N \rightarrow \infty$, but past the $\lambda_0/2$ density threshold adding more satellites becomes less crucial.

Figure 4 plots the required number of satellites N and the scattering crosssection $\bar{\sigma}_b$ of the bare object versus a for

$\overline{\text{RCS}} = -30$ dB. As expected, N increases with a . Interestingly, just as for $\bar{\sigma}_b$, this increase is perfectly linear, showing that the number of satellites required to achieve a particular level of scattering reduction increases in proportion to the object size. This observation can be further explained, shedding additional insights into the dependence of RCS on N , by looking at the effect of cloaking on the coefficients of the cylindrical harmonics of the scattered field. The goal of any cloaking scheme is to cancel as many of these coefficients as possible. For the case under study, these coefficients are given by

$$C_n = I_n + X_n \sum_{k=1}^N I_k e^{-jn\phi_k}, \quad (15)$$

consistent with Eq. (8). Figure 5 shows these coefficients without and with cloaking satellites for $a = \lambda_0/2$ and different N . In the case of the bare object, $|C_n|$ decreases rapidly as n increases beyond a particular value n^* . An estimation of this value can be obtained from the asymptotic formula of $|C_n|$ for large n :

$$|C_n| \sim E_0 \sqrt{\frac{1}{2\pi\beta_0}} \left(\frac{e\beta_0 a}{2n} \right)^{2n}. \quad (16)$$

From this equation, we can see that for $n > n^* = e\beta_0 a/2$, $|C_n|$ decreases faster than exponentially with increasing

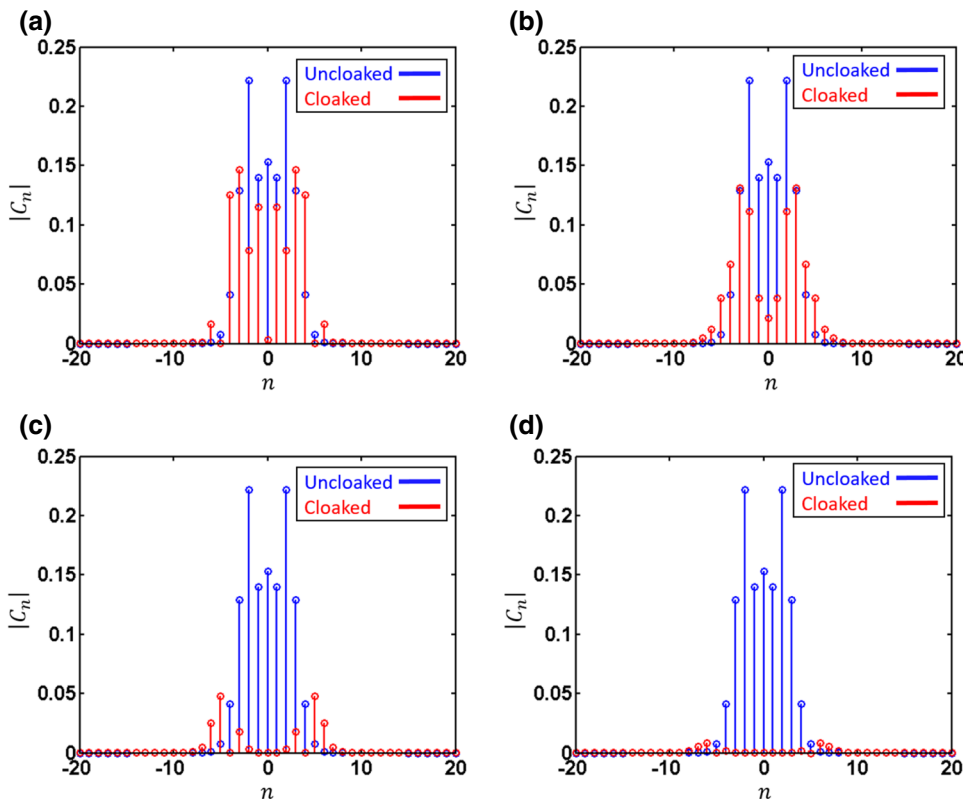


FIG. 5. Magnitude of the scattering harmonics with and without cloaking for $a = \lambda_0/2$ and different numbers of the satellites: (a) $N = 2$, (b) $N = 5$, (c) $N = 8$, and (d) $N = 10$.

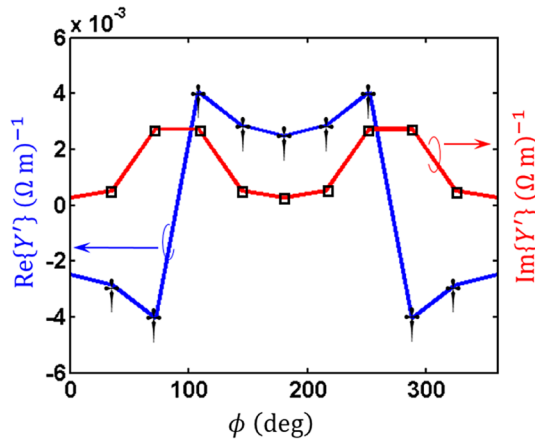


FIG. 6. Optimal values of the modified wire admittance Y'_k at f_0 for $a = \lambda_0/2$, $r_c = a + 0.05\lambda_0$ and $N = 10$.

n . For $a = \lambda_0/2$, the critical value of n is 5, which is in good agreement with the data in Fig. 5. If N , i.e., the number of cloaking elements, is smaller than n^* , there are not enough degrees of freedom to cancel all relevant harmonics of the bare cylinder, as seen in Figs. 4(b) and 5(a). In fact, some of the higher-order coefficients actually increase, which is not surprising since the cancellation is targeted in an average sense. This behavior results in a slow decrease of $\overline{\text{RCS}}$ with increasing N for small values of N , also consistent with Fig. 3. On the other hand, if $N > n^*$, we have enough degrees of freedom to cancel the dominant harmonics and also several other harmonics. Furthermore, since the amplitude of the less relevant harmonics decreases quickly with their order, a larger N results in a fast decrease of $\overline{\text{RCS}}$, as observed in Fig. 3 for a large N . It is evident from the above discussion that n^* approximately provides the number of elements N^* at the kneepoint in Fig. 3. Indeed, it can be found from Fig. 3 that $n^* = 0.68N^*$. This discussion shows the feasibility of cloaking arbitrarily large objects with reasonable complexity using the presented active cloak.

As already mentioned at the beginning of this section, the loaded wires can be modeled through the boundary condition $I_k = Y_k E_k$, from which, having found I_k , we can calculate Y_k and subsequently the lumped admittances

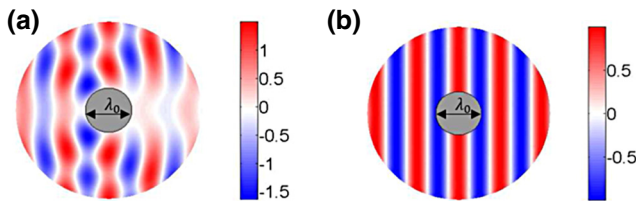


FIG. 7. Total electric field distribution (normalized to E_0) for the same parameters as in Fig. 6: (a) Without cloaking satellites. (b) With cloaking satellites.

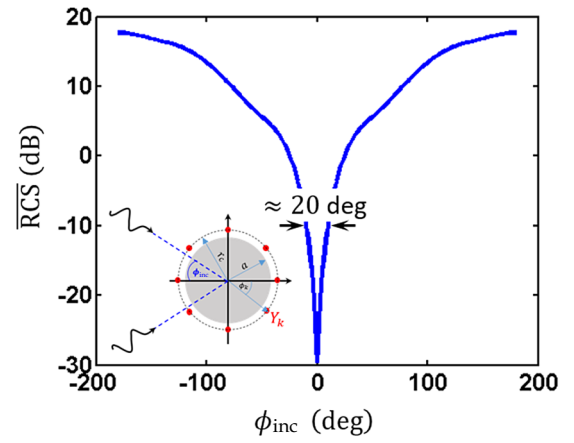


FIG. 8. Normalized scattering coefficient $\overline{\text{RCS}}$ versus the angle of incidence ϕ_{inc} at f_0 for the same parameters as in Fig. 6.

$Y_{L,k} = Y_k/d$. Nevertheless, this boundary condition contains an inherent difficulty: the induced electric field by a line source itself, such as a thin wire, is singular at the source location, thereby leading to a similar singularity for E_k . This problem is similar to the singularity encountered in the definition of polarizability of point dipoles, and it can be resolved as follows. Consider E_k^{ind} to be the induced electric field by the k th wire on itself and E_k^{loc} to be the local field on the k th wire due to the incident wave and all the other radiating sources, where both are calculated in the presence of the cylinder. Then, the total field on the k th wire is given by $E_k = E_k^{\text{ind}} + E_k^{\text{loc}}$ and the required admittance at this element can be calculated as

$$\frac{1}{Y_k} = \frac{1}{\alpha_k} + \frac{E_k^{\text{ind}}}{I_k}, \quad (17)$$

where $\alpha_k = I_k/E_k^{\text{loc}}$ is defined as the polarizability of the k th satellite, I_k is depicted in Fig. 2, and E_k^{loc} is

$$\begin{aligned} E_k^{\text{loc}} = & E^{\text{inc}}(r_c, \phi_k) + E^{s,b}(r_c, \phi_k) \\ & - \frac{\beta_0 \eta_0}{4} \sum_{\substack{m=1 \\ m \neq k}}^N \sum_{n=-\infty}^{\infty} I_m H_n^{(2)}(\beta_0 r_c) \\ & \left[J_n(\beta_0 r_c) - \frac{J_n(\beta_0 a)}{H_n^{(2)}(\beta_0 a)} H_n^{(2)}(\beta_0 r_c) \right] e^{jn(\phi_k - \phi_m)}. \end{aligned} \quad (18)$$

Equation (18) takes into account the interference at the k th satellite from all other wires and it also shows that E_k^{loc} is bounded, therefore, no problem exists in calculating α_k . On the other hand, E_k^{ind} is singular and the term E_k^{ind}/I_k requires special care. The real part of this term can be

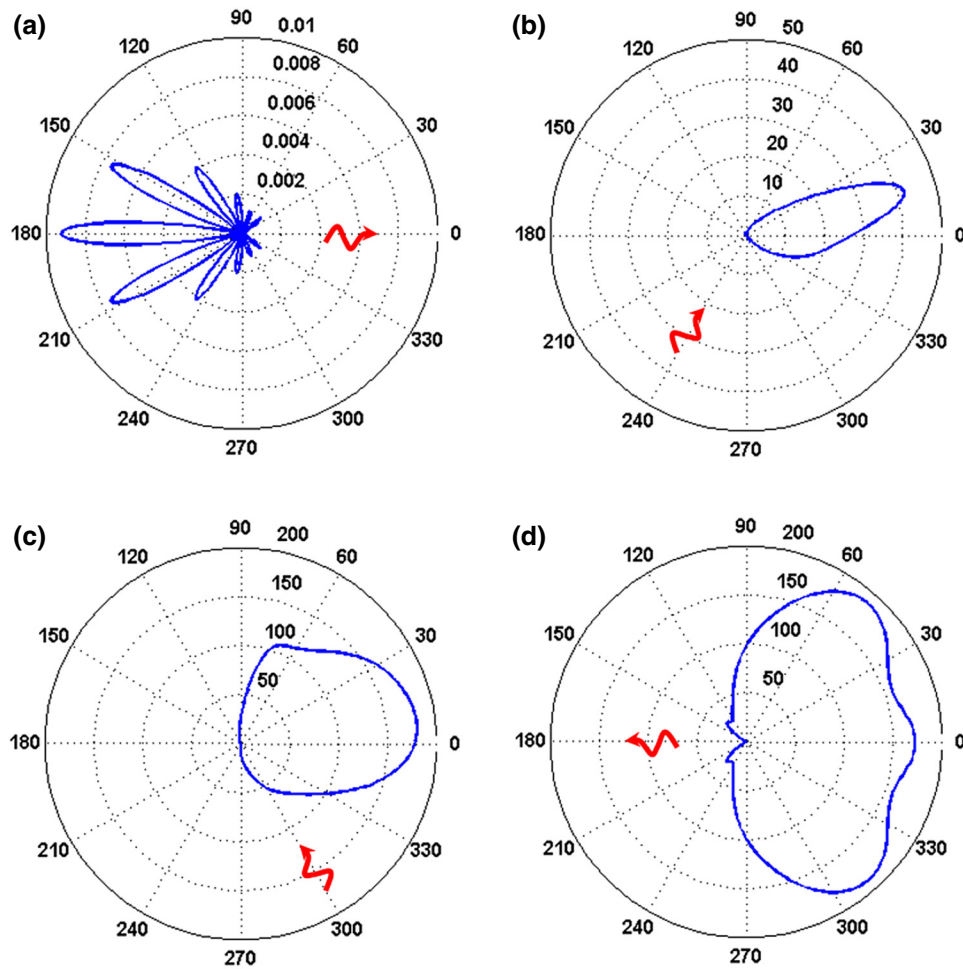


FIG. 9. Cloaked scattering crosssection $\bar{\sigma}_c$ versus the azimuthal angle ϕ for different angles of incidence: (a) $\phi_{inc} = 0^\circ$, (b) $\phi_{inc} = 60^\circ$, (c) $\phi_{inc} = 120^\circ$, and (d) $\phi_{inc} = 180^\circ$. The parameters of the structure are the same as in Fig. 6.

calculated by writing it as

$$\text{Re} \left\{ \frac{E_k^{\text{ind}}}{I_k} \right\} = \frac{2}{|I_k|^2} \frac{1}{2} \text{Re} \{ E_k^{\text{ind}} I_k^* \} \quad (19)$$

and noting that $(1/2)\text{Re}\{E_k^{\text{ind}} I_k^*\}$ is the opposite of the radiated power by a line source with current I_k . This power is essentially given by Eq. (11) with only a single term in the sum with respect to k and without the term l_n :

$$\text{Re} \left\{ \frac{E_k^{\text{ind}}}{I_k} \right\} = -\frac{2\pi}{\eta_0} \sum_{n=-\infty}^{\infty} |X_n|^2. \quad (20)$$

In order to calculate the imaginary part of E_k^{ind}/I_k , we assume that the wire has a finite but small radius ρ_0 . Then, on the surface of the wire, E_k^{ind} is approximately equal to

$$E_k^{\text{ind}} \approx -\frac{\beta_0 \eta_0}{4} I_k H_0^{(2)}(\beta_0 \rho_0) + \frac{\beta_0 \eta_0}{4} I_k \sum_{n=-\infty}^{\infty} \frac{J_n(\beta_0 a)}{H_n^{(2)}(\beta_0 a)} [H_n^{(2)}(\beta_0 r_c)]^2, \quad (21)$$

which can be obtained from Eq. (5). In deriving Eq. (21), we have used the identity

$$H_0^{(2)}(\beta_0 |\rho - \rho'|) = \sum_{n=-\infty}^{\infty} H_n^{(2)}(\beta_0 \rho) J_n(\beta_0 \rho') e^{jn(\phi - \phi')} \quad (22)$$

and assumed that $\rho_0 \ll r_c$, so that the effect of the wire radius can be neglected in the second term of Eq. (21), which provides the scattered field of the dipole by the cylinder. From this equation, we find that the dominant term of $\text{Im}\{E_k^{\text{ind}}/I_k\}$ is $-(\beta_0 \eta_0/4) Y_0(\beta_0 \rho_0)$, where $Y_n(x)$ is the Bessel function of the second kind and n th order, which for $\rho_0 \rightarrow 0$ is approximately equal to $-[(\beta_0 \eta_0)/(2\pi)] \ln(\beta_0 \rho_0)$. Therefore, we get

$$\frac{E_k^{\text{ind}}}{I_k} = i \frac{\beta_0 \eta_0}{2\pi} \ln(\beta_0 \rho_0) - \frac{2\pi}{\eta_0} \sum_{n=-\infty}^{\infty} |X_n|^2. \quad (23)$$

The physical meanings of the real and imaginary parts of E_k^{ind}/I_k are the radiation resistance and the parasitic reactance of a thin wire, respectively. Notice that the reactance depends on the wire radius ρ_0 . In practice, this radius is an

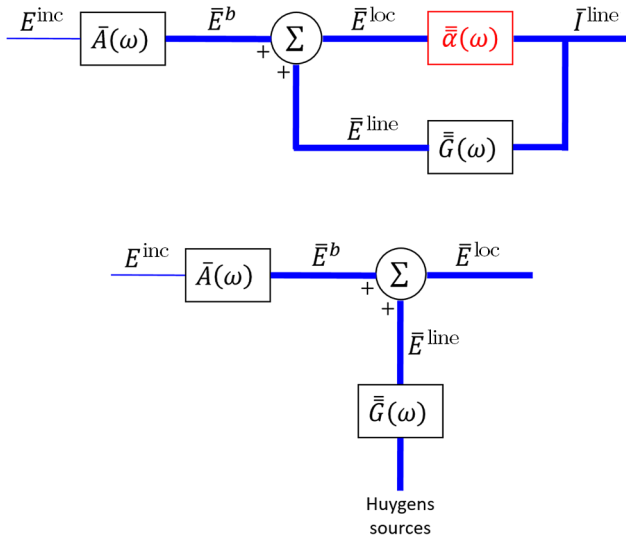


FIG. 10. (a) Closed-loop feedback MIMO model for the proposed PT cloak. (b) Open-loop MIMO model for the active cloak in Ref. [24].

effective quantity that depends on the actual shape and size of the satellite antennas. Furthermore, the nonidealities of the discrete or integrated components used in implementing the lumped admittances $Y_{L,k}$ will have an effect on Y_k . These parasitic effects can be absorbed in the design of Y_k . Hence, in order to simplify the analysis, we define a modified wire admittance Y'_k as

$$\frac{1}{Y'_k} = \frac{1}{Y_k} + i \frac{\beta_0 \eta_0}{2\pi} \ln(\beta_0 \rho_0). \quad (24)$$

From Eq. (23), it follows that

$$\frac{1}{Y'_k} = \frac{E_k^{\text{loc}}}{I_k} - \frac{2\pi}{\eta_0} \sum_{n=-\infty}^{\infty} |X_n|^2. \quad (25)$$

Figure 6 shows the real and imaginary parts of Y'_k for the same parameters as in Fig. 2. It can be seen that the admittance profile is indeed PT symmetric in the sense that satellites at symmetric positions with respect to the y axis ($\phi = 90^\circ$) have the same imaginary part and opposite real parts. As mentioned in the introduction, this PT symmetric property can be intuitively understood as the operation of a cloak that is ideally absorbing the incident wave on the passive side of the object (like a stealth surface), and re-emitting it on the active side through gain (operating the time-reversed operation of an ideal stealth surface). The lossy side can be implemented using passive elements, which, in principle, is very similar to conventional stealth technologies. The gain side, on the other hand, requires the use of active circuits. Possible implementation for both the lossy and gain sides will be provided in the next section. Figure 7 shows the total electric field distribution at the

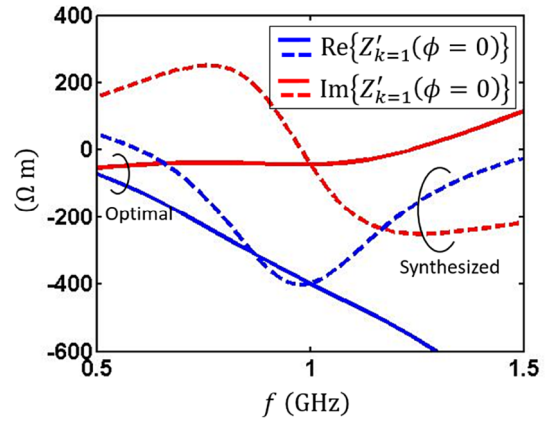


FIG. 11. Optimal dispersion (solid) for the gain element at $\phi = 0^\circ$ to maintain a flat 30-dB reduction compared to the actual dispersion (dashed) achieved with the circuit implementation in Fig. 12(b).

design frequency with and without cloaking for the case study under consideration. These fields are analytically calculated by substituting the current profile in Fig. 2, or equivalently the admittance profile in Fig. 6, into Eqs. (4) and (5). Clearly, the object becomes almost ideally undetectable in the cloaked scenario for which all scattering is suppressed, as opposed to conventional passive stealth technologies for which only backward scattering (reflection) is suppressed and a large shadow exists.

Although in this paper we focus on unidirectional cloaking, it is still important from a practical perspective that the cloak works well within a certain angular beam width. The angular width is defined as the range of incident angles where $\overline{\text{RCS}}$ stays above a particular value. For a -10 dB threshold, the achieved angular width is 20° in this design, as seen in Fig. 8, which depicts $\overline{\text{RCS}}$ vs the incidence angle ϕ_{inc} . For $|\phi_{\text{inc}}| \geq 25^\circ$, $\overline{\text{RCS}}$ becomes larger than 0 dB, meaning that the cloaked object scatters more than the bare object. Maximum scattering occurs for $\phi_{\text{inc}} = 180^\circ$, when the structure is illuminated from its gain side. This is also visible in Fig. 9, presenting the radiation pattern of the structure for different incidence angles. However, it is interesting to notice that backward scattering in the $-x$ direction is zero, regardless of the incident angle. As explained in Ref. [38], this fundamentally lies in reciprocity: since the scattered field for $\phi_{\text{inc}} = 0^\circ$ is zero for any observation angle, the same should hold for the scattered field in the $-x$ direction for any angle of incidence. Notice the very different scales in the different panels of Fig. 9.

III. STABILITY ANALYSIS AND TRANSIENT RESPONSE

As for any feedback system incorporating active circuitry, the stability and transient dynamics of the proposed

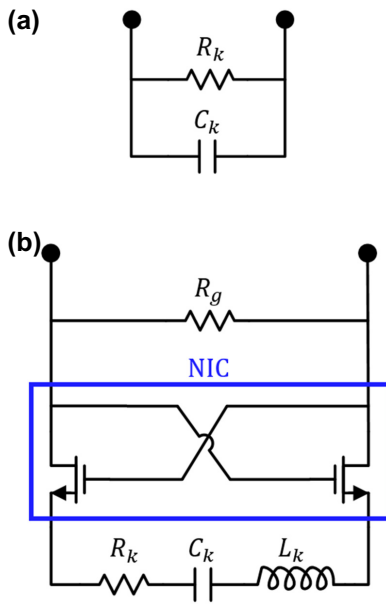


FIG. 12. Circuit implementation of the k th satellite. (a) Passive side. (b) Gain side. A simplified schematic (dc biasing is not shown) for the NIC circuit is also shown using two cross-coupled CMOS transistors [40,41].

cloak should be examined carefully. While the previous results show that in steady-state at the design frequency the scattering also stays finite for excitation from the active side, stability cannot be firmly answered through a frequency-domain analysis, but requires analyzing the impulse response of the structure, i.e., excitation with a short pulse in the time domain. Since the frequency content of such a pulse is infinite, it is necessary to consider the frequency dispersion of the lumped admittance $Y_{L,k}$ of the wire satellites, or equivalently the frequency dispersion of the modified wire admittances Y'_k defined in Eq. (24). Then, the question of stability can be modified into whether there is a physically realizable frequency dispersion for Y'_k that makes the cloak inherently stable. Specifying the dispersion will also determine the cloaking bandwidth, showing

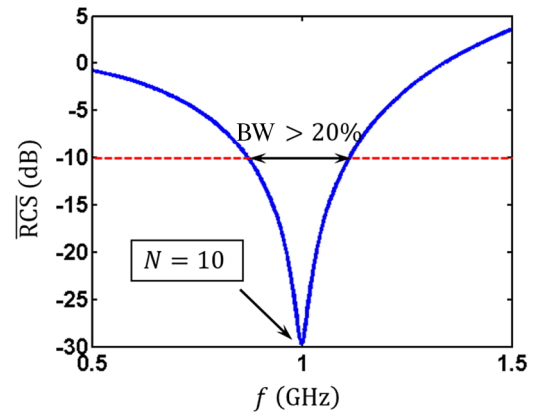


FIG. 14. Scattering coefficient \overline{RCS} vs frequency for the same parameters as in Fig. 13(b).

that, for active feedback systems, the ultimate limitation in bandwidth is stability.

Interestingly, the proposed cloak can be precisely modeled as a feedback system, which not only facilitates its stability analysis through basic control theory principles, but also provides insights into its dynamics. Such a feedback model is presented in Fig. 10(a), and can be developed as follows. Consider an incident EM pulse E^{inc} propagating toward the object along the design direction. This pulse is scattered by the object, resulting in a field E_k^b at the position of the k th wire. This scattering process can be described through a first-rank operator (vector) \bar{A} as $\bar{E}^b = \bar{A}E^{\text{inc}}$, where \bar{E}^b is the column vector with elements E_k^b . The fields E_k^b drive currents $I_k = \alpha_k E_k^b$ through the wires, a process described through the diagonal polarizability tensor $\bar{\alpha}$, whose elements are the satellite polarizabilities α_k , as $\bar{I} = \bar{\alpha}\bar{E}^b$, where \bar{I} is the column vector of I_k . The induced currents on the wires start radiating, leading to an additional electric field E_k^{line} at the position of the wires, which are related to the currents through the Green function operator \bar{G} as $\bar{E}^{\text{line}} = \bar{G}\bar{I}$, where \bar{E}^{line} is the column vector of E_k^{line} . These additional fields should be added to E_k^b when calculating I_k , highlighting the feedback

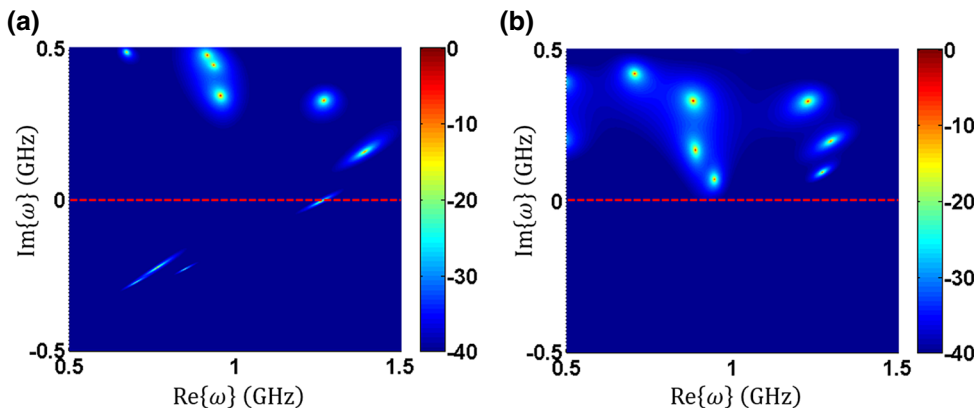


FIG. 13. Stability function $H(\omega)$ as defined in Eq. (33) where the bright spots correspond to the poles of the system for different values of Q : (a) $Q = 0.1$ where unstable poles can be found in the lower-half plane. (b) $Q = 0.5$ where all poles lie in the upper-half plane indicating stability.

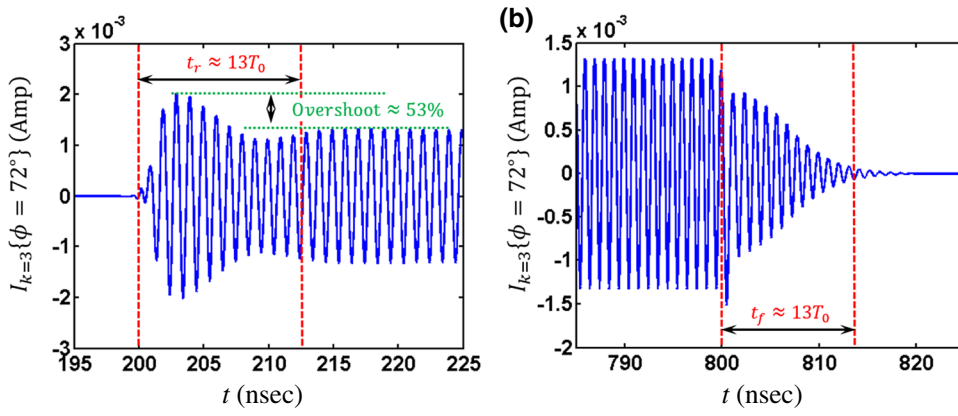


FIG. 15. Transient response of the generated current in the gain element at $\phi = 72^\circ$ due to an incident plane wave carrier, the amplitude of which is digitally modulated by an on-off pulse: (a) Rising edge of the envelope. (b) Falling edge of the envelope.

mechanism. Combining all these processes leads to the closed-loop feedback model in Fig. 10(a). Notice that the feedback action performed by this loop through the Green function $\bar{\bar{G}}$ and the polarizability tensor $\bar{\bar{\alpha}}$ is a combination of both positive and negative feedback responses, through the active and passive elements, respectively. If the phase accumulated by the signal radiated by any of the gain elements as it propagates around the loop is $2m\pi$, where m is an integer, the system will oscillate. In order to avoid this scenario and ensure the cloak's stability, the cross-coupling between the active and lossy elements must guarantee that the loop gain seen by the currents flowing through the active satellites is slightly less than unity at all frequencies, hence oscillations, if any, are not sustained. In other words, the negative and positive feedback actions, or the embodied loss and gain, must be balanced. From control theory, a necessary and sufficient condition to achieve this goal is to make sure that all poles of the loop transfer matrix fall in the upper half of the complex frequency spectrum. This condition can be satisfied by engineering the dispersion of the satellite admittances properly as we illustrate next. First, the currents through the wires are calculated from the developed model in Fig. 10(a) as follows:

$$\bar{I} = (\bar{U} - \bar{\bar{\alpha}}\bar{\bar{G}})^{-1}\bar{\bar{\alpha}}\bar{A}E^{\text{inc}}, \quad (26)$$

where \bar{U} is the identity matrix. From this equation, we define the closed-loop transfer matrix

$$\bar{\bar{T}} = (\bar{U} - \bar{\bar{\alpha}}\bar{\bar{G}})^{-1}\bar{\bar{\alpha}}. \quad (27)$$

Since \bar{A} is not part of the closed loop, it does not impact stability, and for this reason it has not been included in Eq. (27). Interestingly, the active cloak in Ref. [24] is a special case of the one discussed here. In fact, it is the open-loop scenario of our system, as shown in Fig. 10(b), where the required currents (designated as Huygen's sources in Ref. [24]) are externally preset for a particular, known *a priori*, excitation. As we explained in the Introduction, this predetermined cloak is detectable

under illumination with pulsed or modulated signals. In order to track the variations of the incident signal, should they be amplitude, frequency, and/or phase modulation, a control loop is required. Ref. [23] provides this loop through an active sensing/feeding network and complex signal processing, which makes it slow, and therefore, limits the BW and operation frequency. On the other hand, in the PT symmetric cloak proposed herein, this loop is automatically achieved through the feedforward polarizability tensor $\bar{\bar{\alpha}}$, describing the lumped admittances loading the satellites.

In the previous section, we showed how we can calculate the admittance values in order to achieve a particular scattering reduction (30 dB) at a given frequency f_0 . If we follow the same procedure at different frequency points, we can find the optimal dispersion of all elements to maintain the same level of scattering reduction over frequency. As an example, Fig. 11 shows the optimal dispersion ($Z'_{k=1} = 1/Y'_{k=1}$) for the gain element at $\phi = 0^\circ$ in order to obtain $\text{RCS} = -30$ dB over the entire band depicted in this figure. A cloak with such a dispersion is very similar to an ideal bandstop filter with flat isolation over frequency. As in any practical filter design, there is a limitation on the maximum bandwidth to maintain a certain level of isolation, as imposed by the Bode-Fano criterion [39]. The problem of cloaking is very similar, and Fig. 11 leads to the same conclusion, since the required real part of the admittances at the gain side has to be negative at all frequencies, which is not physically possible. Therefore, the bandwidth in this case is limited to the range over which a stable negative resistance can be realized. Nevertheless, this optimal dispersion is still useful as a design guideline, i.e., we can synthesize the admittance elements to be as close as possible to this profile in order to maximize the cloaking bandwidth. Our realistic stable design, introduced next, synthesizes the dispersion shown with dashed lines in Fig. 11.

The passive side of the cloak can be implemented using a basic parallel RC circuit, as shown in Fig. 12(a). The active side, on the other hand, requires the use of resonant circuits in conjunction with a negative impedance

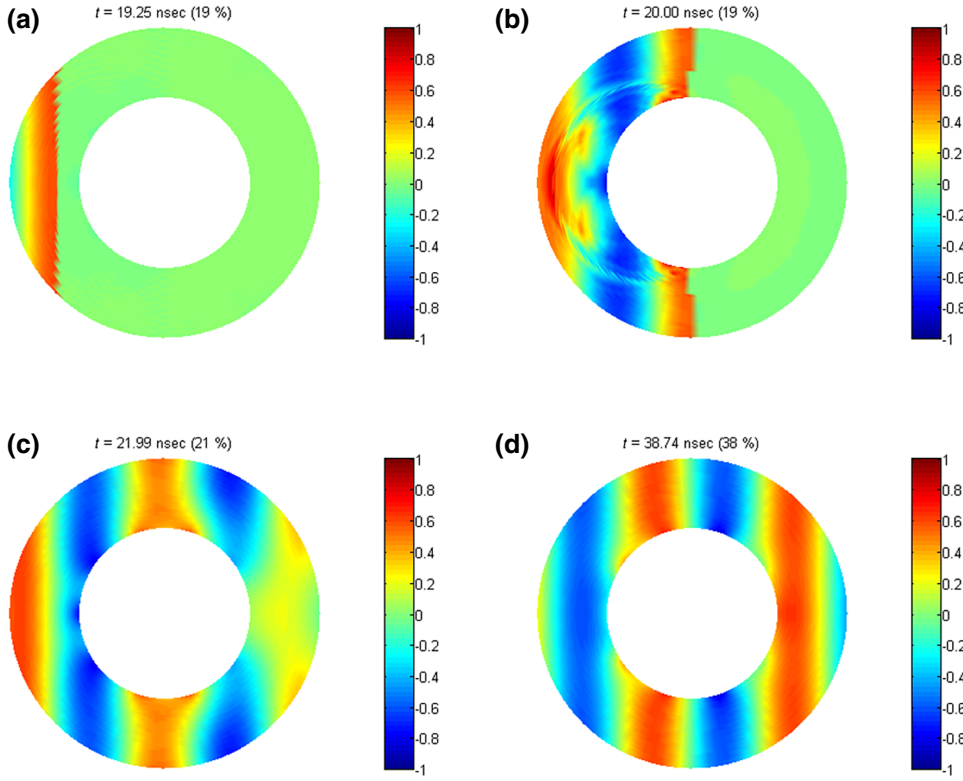


FIG. 16. Snapshots for the total electric field (normalized to E_0) at the rising edge of an amplitude-modulated sinusoidal signal impinging on a cloaked PEC cylinder with radius $a = \lambda_0/2$.

converter (NIC) [40,41]. NICs are active circuits that provide a non-Foster frequency dispersion. They were applied in Ref. [42] to broaden the cloaking BW by synthesizing a homogeneous metasurface cloak with negative frequency dispersion that compensated the positive dispersion of the scattering from the object it concealed. Here, on the contrary, we apply them to synthesize the proposed PT symmetric cloak, with advantages in terms of stability and overall dynamics of the response. Figure 12(b) shows a first-order realization that employs a series RLC resonant tank loading an NIC circuit consisting of two cross-coupled CMOS transistors (dc biasing is not shown for simplicity) in parallel with a constant resistance $R_g = 100 \Omega$ that provides a further degree of freedom to control the overall dispersion. The details of the NIC circuit design are beyond the scope of this paper, and we assume here an ideal NIC with a transformation factor of -1 over the cloaking BW. It should be stressed that the NIC will always be dispersive in practice, and the transformation factor is eventually expected to be positive far from the center frequency. Yet, assuming that this occurs beyond the desired cloaking BW, the assumption of an ideal inband NIC is reasonable to simplify the analysis. The required values of the lumped elements in Fig. 12 can be calculated as follows: for the passive side, i.e., $-90^\circ < \phi_k < 90^\circ$,

$$R_k = 1/\text{Re}\{Y_{L,k}\}, \quad (28)$$

$$C_k = \text{Im}\{Y_{L,k}\}/\omega_0, \quad (29)$$

while for the active side, i.e., $90^\circ < \phi_k < 270^\circ$,

$$R_k = \left[1 + \left(\frac{R_g - \text{Re}\{Z_{L,k}\}}{\text{Im}\{Z_{L,k}\}} \right)^2 \right] \frac{\text{Im}\{Z_{L,k}\}/\text{Im}\{Y_{L,k}\}}{(R_{2,k} - \text{Re}\{Z_{L,k}\})}, \quad (30)$$

$$L_k = R_k/(\omega_0 Q_k), \quad (31)$$

$$C_k = \frac{1}{\omega_0} \left[\frac{1}{\omega_0 L_k} - \frac{\text{Im}\{Y_{L,k}\}}{1 + \left(\frac{R_g - \text{Re}\{Z_{L,k}\}}{\text{Im}\{Z_{L,k}\}} \right)^2} \right], \quad (32)$$

where $Z_{L,k} = 1/Y_{L,k}$ and Q_k is the quality factor of the k th resonance on the gain side. It is important to highlight that the role of the NIC here is not to generate a negative capacitance or reactance, as in most of the cases where bandwidth extension is sought, an operation which is notorious for stability problems due to the fact that a negative capacitance or reactance in the presence of any parasitic resistance results in an unstable pole in the lower-half frequency plane [43,44]. On the other hand, here, NIC inverts the total admittance of a series resonant circuit without affecting its poles. Also, thanks to the feedback action of the loop in Fig. 10(a), any unstable pole that may arise due to parasitics, which always exist in practical scenarios, can still be stabilized. Therefore, we expect that the circuit in Fig. 12(b), when used in the proposed feedback cloak, will be immune to stability issues.

Having determined the dispersion of the circuit elements, we can now impose stability by requiring that all

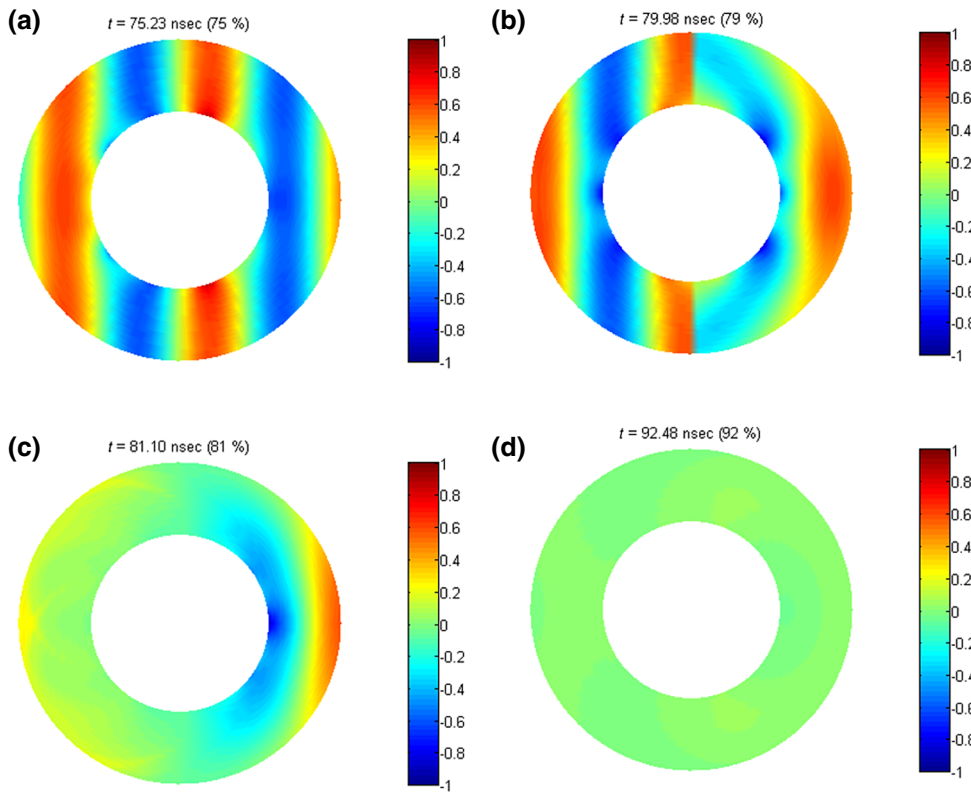


FIG. 17. Snapshots for the total electric field (normalized to E_0) at the falling edge of an amplitude-modulated sinusoidal signal impinging on a cloaked PEC cylinder with radius $a = \lambda_0/2$.

poles of each element in the transfer matrix \bar{T} lie in the upper half of the complex frequency plane. To find these poles, we define the stability function

$$H(\omega) = \sum_{i=1}^N \sum_{j=1}^N |T_{ij}(\omega)|, \quad (33)$$

which contains the union of all poles, and we plot it in the complex frequency. To simplify the next design steps, we assume that all the resonant tanks on the gain side have the same quality factor Q , and calculate the values of the lumped elements accordingly.

Figure 13 shows $H(\omega)$ in the complex frequency plane for two different values of Q . For values as small as 0.1, the frequency range over which the active impedance is negative is excessively large, leading to an unstable system with poles in the lower-half plane. Increasing Q reduces the range where the real part of the impedance is negative and it gradually pushes the operation into a stable regime. As shown in Fig. 13(b), $Q = 0.5$ is sufficient to achieve this goal and maintain stability. As one may expect, increasing Q further can push the poles further away from the real axis into the stable upper-half plane, thus providing larger immunity against inevitable random variations in practical implementations. However, this comes at the expense of reducing the cloaking BW. Therefore, it is a matter of design to choose the appropriate value of Q depending on

the given specifications for a particular application. In this paper, we use $Q = 0.5$ to maximize the cloaking BW.

The achieved cloaking bandwidth can be calculated from Fig. 14, which shows the scattering reduction \overline{RCS} vs frequency for the synthesized dispersion in Fig. 12. By using the same analogy with bandstop filters, the cloaking bandwidth is defined as the frequency range where scattering reduction stays above some percentage of the peak value. For a -10 dB threshold, the fractional BW is larger than 20%, and it can be potentially increased further by employing well-established multiresonant techniques commonly used in wideband filters and matching networks [45], under the conditions of stability and causality [46].

Further insights into the cloaking mechanism can be obtained by studying the transient response of the system for an incident plane wave carrier, the amplitude of which is digitally modulated by an on-off pulse. We first calculate the transient response of the currents flowing through the wires surrounding the object by finding the Fourier transform $E^{\text{inc}}(\omega)$ of the incident pulse, then calculating the Fourier transform of the currents through Eq. (26), and finally evaluating the inverse Fourier transform of $\bar{T}(\omega)$. Figure 15 presents the time-domain response for the current through the gain element at $\phi = 72^\circ$ on the active side of the cloak, where the negative resistance at f_0 is maximum (Fig. 6). It can be seen that the response is underdamped at the rising edge of the signal envelope, i.e., the cloaked object initially scatters more than the bare cylinder, until it settles at its steady state. This additional

scattering, so-called overshooting, is less than 53% and the settling time to reach less than 1% error is 13 cycles at both the rising and falling edges. This fast underdamped response at the gain side results from the small value of Q of the RLC resonators. At the passive side (not shown here), there is no overshooting and settling is even faster, since there is neither gain nor resonance.

As with the currents, the total fields of the cloaked structure can be calculated first in the frequency domain by using the Fourier transform of the incident pulse, and then transforming the result to the time domain. Figures 16 and 17 show snapshots for the animated total electric field with cloak at the rising and falling edges of the incident modulated pulse, respectively. Figure 16(b) shows that the incident pulse is initially scattered before the cloaking feedback mechanism generates the required currents through the satellites to conceal the object. Then, the passive side of the cloak starts to absorb the incident wave and reduces the scattered power in a way similar to conventional stealth as depicted in Fig. 16(c). Finally, the active side also locks onto the incident wave and starts to re-emit it with the same frequency, phase, and amplitude, cancelling the shadow in a superstealth fashion, as shown in Fig. 16(d).

Similarly, Fig. 17 shows that the active side does not abruptly stop its radiation when the incident wave excitation stops, but rather exponentially decays until the system reaches its new steady state. More importantly, this also proves the system stability, in agreement with our previous results.

IV. DISCUSSION AND CONCLUSIONS

In this paper, we present a practically relevant unidirectional active microwave cloak, inspired by the concept of PT symmetry. The proposed cloak consists of a finite number of thin antennas loaded with external circuits (so-called satellites) that generate the required current profile to cancel the scattered waves from the illuminated object and achieve total invisibility. We establish a systematic approach to optimize the cloak design in analogy with other microwave devices such as bandstop filters. We also develop a feedback model to study the cloak's dynamics and discuss the conditions to maintain stability. As an example, we show how to use this procedure to conceal a circularly symmetric PEC cylinder from an impinging causal-modulated pulse with center frequency at 1 GHz and transverse-magnetic (TM) polarization, resulting in a scattering reduction of 10 dB over a fractional BW larger than 20% and peak reduction of 30 dB at the center frequency.

For simplicity, our analysis here focuses on the cloaking of circular cylinders, but the presented design procedure can be applied to arbitrarily shaped objects and account for inevitable parasitics in actual implementations. We

note that the satellites can be realized using, for example, conventional dipole antennas connected to optimal loads in discrete or integrated form, mounted on printed circuit boards. In order to derive the optimal parameters of these loads, one can follow an analysis analogous to the one presented in this paper, yet based on full-wave simulations. More specifically, the scattering object and the cloak are first simulated, replacing the loads with discrete ports, then the S parameters at all ports are extracted. These network parameters can be used to express the scattered fields as a superposition of the currents flowing through the discrete ports, and then, following a similar procedure as in this paper, the scattered power is minimized to derive the optimal admittances that should be connected at the discrete ports to achieve the target scattering reduction. An extension to also suppress the transverse-electric (TE^z) polarization is viable by surrounding the scattering object with in-plane circular loops loaded with another series of lumped loads.

Compared to passive approaches, the presented cloak offers the possibility of breaking the size bandwidth trade-off of passive, linear metamaterial cloaks. Specifically, the BW herein is only limited by stability on the gain side, which is a less strict requirement than passivity, allowing to achieve 20% fractional BW for a 10-dB scattering reduction of a PEC cylinder with a diameter equal to one wavelength. Such a BW is significantly larger than the one that can be achieved with conventional passive cloaks, based on azimuthally symmetric covers for the same object size [21]. This BW can potentially be further increased by employing well-established multiresonance approaches commonly used in the design of wideband microwave devices, making the proposed approach suitable for radar and communication systems.

ACKNOWLEDGMENTS

This work was supported by the National Science Foundation, the Air Force Office of Scientific Research with MURI grant No. FA9550-18-1-0379, and the Simons Foundation.

-
- [1] J. B. Pendry, D. Schurig, and D. R. Smith, Controlling electromagnetic fields, *Science* **312**, 1780 (2006).
 - [2] U. Leonhardt, Optical conformal mapping, *Science* **312**, 1777 (2006).
 - [3] J. Li and J. B. Pendry, Hiding Under the Carpet: A New Strategy for Cloaking, *Phys. Rev. Lett.* **101**, 203901 (2008).
 - [4] A. Alù, Mantle cloak: Invisibility induced by a surface, *Phys. Rev. B* **80**, 245115 (2009).
 - [5] P.-Y. Chen and A. Alù, Mantle cloaking using thin patterned metasurfaces, *Phys. Rev. B* **84**, 205110 (2011).

- [6] A. Alù and N. Engheta, Achieving transparency with plasmonic and metamaterial coatings, *Phys. Rev. E* **72**, 016623 (2005).
- [7] A. Alù and N. Engheta, Multifrequency Optical Invisibility Cloak with Layered Plasmonic Shells, *Phys. Rev. Lett.* **100**, 113901 (2008).
- [8] P. Alitalo, F. Bongard, J.-F. Zürcher, J. Mosig, and S. Tretyakov, Experimental verification of broadband cloaking using a volumetric cloak composed of periodically stacked cylindrical transmission-line networks, *Appl. Phys. Lett.* **94**, 014103 (2009).
- [9] S. Tretyakov, P. Alitalo, O. Luukkonen, and C. Simovski, Broadband Electromagnetic Cloaking of Long Cylindrical Objects, *Phys. Rev. Lett.* **103**, 103905 (2009).
- [10] Y. Lai, H. Chen, Z.-Q. Zhang, and C. T. Chan, Complementary Media Invisibility Cloak that Cloaks Objects at a Distance Outside the Cloaking Shell, *Phys. Rev. Lett.* **102**, 093901 (2009).
- [11] J. C. Soric, A. Monti, A. Toscano, F. Bilotti, and A. Alù, Dual-polarized reduction of dipole antenna blockage using mantle cloaks, *IEEE Trans. Antennas Propag.* **63**, 4827 (2015).
- [12] A. Monti, J. Soric, A. Alù, A. Toscano, and F. Bilotti, Design of cloaked Yagi-Uda antennas, *EPJ Appl. Metamater.* **3**, 10 (2016).
- [13] A. Monti, J. Soric, M. Barbuto, D. Ramaccia, S. Vellucci, F. Trotta, A. Alù, A. Toscano, and F. Bilotti, Mantle cloaking for co-site radio-frequency antennas, *Appl. Phys. Lett.* **108**, 113502 (2016).
- [14] D. Schurig, J. J. Mock, B. J. Justice, S. A. Cummer, J. B. Pendry, A. F. Starr, and D. R. Smith, Metamaterial electromagnetic cloak at microwave frequencies, *Science* **314**, 977 (2006).
- [15] J. C. Soric, A. Monti, A. Toscano, F. Bilotti, and A. Alù, Multiband and wideband bilayer mantle cloaks, *IEEE Trans. Antennas Propag.* **63**, 3235 (2015).
- [16] N. M. Estakhri and A. Alù, Minimum-scattering superabsorbers, *Phys. Rev. B* **89**, 121416 (2014).
- [17] J. C. Soric, R. Fleury, A. Monti, A. Toscano, F. Bilotti, and A. Alù, Controlling scattering and absorption with metamaterial covers, *IEEE Trans. Antennas Propag.* **62**, 4220 (2014).
- [18] R. Fleury, J. Soric, and Andrea Alù, Physical bounds on absorption and scattering for cloaked sensors, *Phys. Rev. B* **89**, 045122 (2014).
- [19] J. B. Khurgin and A. Boltasseva, Reflecting upon the losses in plasmonics and metamaterials, *MRS Bull.* **37**, 768 (2012).
- [20] F. Monticone and A. Alù, Do Cloaked Objects Really Scatter Less?, *Phys. Rev. X* **3**, 041005 (2013).
- [21] F. Monticone and A. Alù, Invisibility exposed: Physical bounds on passive cloaking, *Optica* **3**, 718 (2016).
- [22] P.-S. Kildal, A. A. Kishk, and A. Tengs, Reduction of forward scattering from cylindrical objects using hard surfaces, *IEEE Trans. Antennas Propag.* **44**, 1509 (1996).
- [23] D. A. B. Miller, On perfect cloaking, *Opt. Express* **14**, 12457 (2006).
- [24] M. Selvanayagam and G. V. Eleftheriades, Experimental Demonstration of Active Electromagnetic Cloaking, *Phys. Rev. X* **3**, 041011 (2013).
- [25] D. L. Sounas, R. Fleury, and A. Alù, Unidirectional Cloaking Based on Metasurfaces with Balanced Loss and Gain, *Phys. Rev. Appl.* **4**, 014005 (2015).
- [26] A. Kord, D. L. Sounas, and A. Alù, in *Proc. IEEE Int. Symp. Ant. and Prop. (APS/URSI)*, July 2016, Fajardo, PR.
- [27] S. A. Cummer, J. Christensen, and A. Alù, Controlling sound with acoustic metamaterials, *Nat. Rev. Mater.* **1**, 16001 (2016).
- [28] X. Chen, Y. Luo, J. Zhang, K. Jiang, J. B. Pendry, and S. Zhang, Macroscopic invisibility cloaking of visible light, *Nat. Commun.* **2**, 176 (2011).
- [29] N. Landy and D. R. Smith, A full-parameter unidirectional metamaterial cloak for microwaves, *Nat. Mater.* **12**, 25 (2013).
- [30] M. Selvanayagam and G. V. Eleftheriades, An active electromagnetic cloak using the equivalence principle, *IEEE Antennas Wireless Propag. Lett.* **11**, 1226 (2012).
- [31] C. M. Bender and S. Boettcher, Real Spectra in Non-Hermitian Hamiltonians Having PT Symmetry, *Phys. Rev. Lett.* **80**, 5243 (1998).
- [32] C. M. Bender, S. Boettcher, and P. N. Meisinger, PT-symmetric quantum mechanics, *J. Math. Phys.* **40**, 2201 (1999).
- [33] C. M. Bender, Making sense of non-Hermitian Hamiltonians, *Rep. Prog. Phys.* **70**, 947 (2007).
- [34] B. Peng, S. K. Özdemir, F. Lei, F. Monifi, M. Gianfreda, G. L. Long, S. Fan, F. Nori, C. M. Bender, and L. Yang, Parity–time-symmetric whispering-gallery microcavities, *Nat. Phys.* **10**, 394 (2014).
- [35] A. Regensburger, C. Bersch, M. A. Miri, G. Onishchukov, D. N. Christodoulides, and U. Peschel, Parity–time synthetic photonic lattices, *Nature* **488**, 167 (2012).
- [36] C. E. Rüter, K. G. Makris, R. El-Ganainy, D. N. Christodoulides, M. Segev, and D. Kip, Observation of parity–time symmetry in optics, *Nat. Phys.* **6**, 192 (2010).
- [37] C. A. Balanis, *Advanced Engineering Electromagnetics* (John Wiley & Sons, Inc., New York, 1989).
- [38] D. L. Sounas and A. Alù, Extinction symmetry for reciprocal objects and its implications on cloaking and scattering manipulation, *Opt. Lett.* **39**, 4053 (2014).
- [39] R. M. Fano, Theoretical limitations on the broadband matching of arbitrary impedances, *J. Franklin Inst.* **249**, 57 (1950).
- [40] B. Razavi, The cross-coupled pair: Part III, *IEEE Solid State Circuits Mag.* **7**, 10 (2015).
- [41] S. E. Sussman-Fort, Gyration-based biquad filters and negative impedance converters for microwaves, *Int. J. RF Microw. Comput.-Aided Eng.* **8**, 86 (1998).
- [42] P. Y. Chen, C. Argyropoulos, and A. Alù, Broadening the Cloaking Bandwidth with Non-Foster Metasurfaces, *Phys. Rev. Lett.* **111**, 23001 (2013).
- [43] E. Ugarte-Munoz, S. Hrabar, D. Segovia-Vargas, and A. Kirichenko, Stability of non-foster reactive elements for use in active metamaterials and antennas, *IEEE Trans. Antennas Propag.* **60**, 3490 (2012).

- [44] J. Brownlie, On the stability properties of a negative impedance converter, [IEEE Trans. Circ. Theory](#) **13**, 98 (1966).
- [45] C. Tang and M. Chen, A microstrip ultra-wideband bandpass filter with cascaded broadband bandpass and bandstop filters, [IEEE Trans. Microw. Theory Techn.](#) **55**, 2412 (2007).
- [46] C. Craeye and A. Bhattacharya, Rule of thumb for cloaking bandwidth based on a wave-packet argument, [IEEE Trans. Antennas Propag.](#) **60**, 3516 (2012).